Conformation of the Substrate and Pterin Cofactor Bound to Human Tryptophan Hydroxylase. Important Role of Phe313 in Substrate Specificity†

Jeffrey McKinney,‡ Knut Teigen,‡ Nils Åge Frøystein,§ Clotilde Salaün,‡ Per M. Knappskog,|| Jan Haavik,‡ and Aurora Martínez*,‡

Department of Biochemistry and Molecular Biology, University of Bergen, Årstadveien 19, N-5009 Bergen, Department of Chemistry, University of Bergen, Allégaten 41, N-5007 Bergen, and Department of Medical Genetics, Haukeland Hospital, University of Bergen, N-5009 Bergen, Norway

Received August 24, 2001; Revised Manuscript Received October 17, 2001

ABSTRACT: Tryptophan hydroxylase (TPH) carries out the 5-hydroxylation of L-Trp, which is the rate-limiting step in the synthesis of serotonin. We have prepared and characterized a stable N-terminally truncated form of human TPH that includes the catalytic domain (Δ90TPH). We have also determined the conformation and distances to the catalytic non-heme iron of both L-Trp and the tetrahydrobiopterin cofactor analogue L-*erythro*-7,8-dihydrobiopterin (BH_2) bound to Δ90TPH by using ^{1}H NMR spectroscopy. The bound conformers of the substrate and the pterin were then docked into the modeled three-dimensional structure of TPH. The resulting ternary TPH·BH_2·L-Trp structure is very similar to that previously determined by the same methods for the complex of phenylalanine hydroxylase (PAH) with BH_2 and L-Phe [Teigen, K., et al. (1999) *J. Mol. Biol. 294*, 807−823]. In the model, L-Trp binds to the enzyme through interactions with Arg257, Ser336, His272, Phe318, and Phe313, and the ring of BH_2 interacts mainly with Phe241 and Glu273. The distances between the hydroxylation sites at C5 in L-Trp and C4a in the pterin, i.e., 6.1 ± 0.4 Å, and from each of these sites to the iron, i.e., 4.1 ± 0.3 and 4.4 ± 0.3 Å, respectively, are also in agreement with the formation of a transient iron-4a-peroxytetrahydropterin in the reaction, as proposed for the other hydroxylases. The different conformation of the dihydroxypropyl chain of BH_2 in PAH and TPH seems to be related to the presence of nonconserved residues, i.e., Tyr235 and Pro238 in TPH, at the cofactor binding site. Moreover, Phe313, which seems to interact with the substrate through ring stacking, corresponds to a Trp residue in both tyrosine hydroxylase and PAH (Trp326) and appears to be an important residue for influencing the substrate specificity in this family of enzymes. We show that the W326F mutation in PAH increases the relative preference for L-Trp as the substrate, while the F313W mutation in TPH increases the preference for L-Phe, possibly by a conserved active site volume effect.

Tryptophan hydroxylase (TPH)[1] is a tetrahydrobiopterin- and non-heme iron-dependent enzyme that hydroxylates L-tryptophan (L-Trp) to 5-hydroxy-L-Trp using (6*R*)-L-*erythro*-5,6,7,8-tetrahydrobiopterin (BH_4) as a cofactor and molecular oxygen as an additional substrate. This is the rate-limiting step in the synthesis of 5-hydroxytryptamine (serotonin) and the initial and uncommitted step in the biosynthesis of melatonin. Together with tyrosine hydroxylase (TH) and phenylalanine hydroxylase (PAH), TPH makes a superfamily of aromatic amino acid hydroxylases, catalyzing key steps in important metabolic pathways (*1*−*3*). These tetrameric enzymes are organized in a regulatory N-terminal domain, a catalytic domain, and a C-terminal oligomerization domain, and they exhibit extensive sequence similarity at the catalytic domains.

Due to the scarcity of the enzyme in animal tissues and its instability in vitro, TPH is the least characterized enzyme of the three aromatic amino acid hydroxylases. Although significant progress has been reported recently on the structural characterization of both TH (*4*) and PAH (*5*−*7*), the three-dimensional (3D) structure of TPH is still not known. The difficulties encountered in the crystallization of this enzyme seem to be related to its instability and insolubility, notably when it is expressed in bacterial systems (*8*). However, the catalytic domain of the enzyme from different sources, including the human brain, appears to be more stable, and several groups have reported its purification and characterization (*9*). Recently, stable full-length TPH forms from the human pineal gland (*10*) and the human parasite *Schistosoma mansoni* (*11*) have been cloned, expressed, and successfully isolated. The first observable product from the pterin cofactor in the TPH reaction is a 4a-hydroxytetrahydropterin, in which the oxygen atom at

† This work was supported by the Research Council of Norway, The Locus on Neuroscience (University of Bergen), and Meltzer L. Høyskolefond.

* To whom correspondence should be addressed. Telephone: 47 55 58 64 27. Fax: 47 55 58 64 00. E-mail: aurora.martinez@ibmb.uib.no.
‡ Department of Biochemistry and Molecular Biology.
§ Department of Chemistry.
|| Department of Medical Genetics, Haukeland Hospital.

[1] Abbreviations: BH_2, L-*erythro*-7,8-dihydrobiopterin; BH_4, (6*R*)-L-*erythro*-5,6,7,8-tetrahydrobiopterin; DTT, dithiothreitol; Δ90TPH, human tryptophan hydroxylase lacking the 90 N-terminal residues; EK, enterokinase; PAH, phenylalanine hydroxylase; TH, tyrosine hydroxylase; TNOESY, transferred NOESY; TPH, tryptophan hydroxylase.

10.1021/bi015722x CCC: $20.00
Published on Web 11/30/2001

position 4a is derived from molecular oxygen (*10*, *12*), as previously detected in the TH- and PAH-catalyzed reactions (*2*, *13*, *14*). This finding, in addition to the sequence similarities at the catalytic domains of the aromatic amino acid hydroxylases, indicates that they have a similar reaction mechanism. Although TPH and PAH and their N-terminally truncated forms hydroxylate both L-Phe to L-Tyr and L-Trp to 5-hydroxy-L-Trp, the enzymes are unable to hydroxylate L-Tyr.

We have recently reported the solution structure of L-Phe and L-*erythro*-7,8-dihydrobiopterin (BH_2), an oxidized inactive cofactor analogue competitive with BH_4, bound to PAH (*15*). In that structure, the cofactor analogue π-stacks with the conserved Phe254, and the O4 atom is located 2.6 ± 0.3 Å from the iron at the active site. This distance is compatible with a proposed coordination of the pterin to the metal and a catalytic mechanism in which the tetrahydropterin cofactor directly donates an electron to the iron which can then bind and activate dioxygen. Recent kinetic and modeling studies on the binding of several cofactor analogues to recombinant human TH have also indicated that the orientation of the pterin complexed with this enzyme in solution is in agreement with that found for the PAH·BH_2 complex (*16*).

In this work, we have studied the conformation of L-Trp and BH_2 bound to the catalytic domain of human TPH (Δ90TPH) by using NMR and docking methods similar to those which have previously been applied to the PAH·BH_2·L-Phe complex (*15*). In the case of the PAH·BH_2 complex, it has previously been shown that the NMR/docking structure corresponds well to the crystal structure (*17*). The high level of sequence identity between the three mammalian hydroxylases, notably, at the catalytic domains, allows the preparation of structural models for TPH (*3*, *18*), and the solution conformations for the bound ligands obtained by NMR have been docked into the modeled structure of TPH. The resulting ternary TPH·BH_2·L-Trp structure is very similar to that previously determined for the PAH·BH_2·L-Phe complex. Despite the similarities, some nonconserved residues are localized at the substrate and pterin binding sites. Phe313 in TPH, which corresponds to Trp326 in PAH, is among the changes that have been found. In this work, we have reversed these changes and shown that this residue is an important predictor of the substrate specificity.

EXPERIMENTAL PROCEDURES

Construction of the pThioHis-TPH Vector and Expression and Purification of Recombinant Δ90TPH, Δ90TPH-F313W, PAH, and PAH-W326F. A construct encoding an amino-terminally truncated form of human TPH lacking the 90 first amino acids was constructed by PCR. A *Kpn*I restriction site was introduced into the human TPH cDNA using the mutant primer (5′-GTT CTC TCT GTG AAG GTA CCA-3′) and a vector specific reverse primer (5′-TGT GAG CGG ATA ACA ATT-3′). This fragment was cloned into the *Kpn*I−*Xba*I sites of the pThioHisB vector (Invitrogen), which allows in-frame fusion with HP-thioredoxin (HP-Trx) and an enterokinase (EK) cleavage site. The F313W mutation was introduced into the pThioHis-Δ90TPH vector using the primers 5′-GCA ACG TGC TAC TGG TTC ACT GTG GAG TTT-3′ and 5′-AAA CTC CAC AGT GAA CCA GTA GC CGT TGC-3′ by the Quick Change kit (Stratagene). All positive clones were sequenced to verify mutagenesis and to exclude other mutations due to *Taq* DNA polymerase misincorporations. The HP-Trx−$(pep)_{EK}$−Δ90TPH and HP-Trx−$(pep)_{EK}$−Δ90TPH-F313W fusion proteins were expressed in the pThioHis B system in *Escherichia coli* TOP10 (Invitrogen). TOP10 cells containing the pThioHisTPH vector were grown at 37 °C in Luria-Bertani medium containing ampicillin (50 μg/mL). Overexpression of TPH was induced with 0.5 mM isopropyl thio-β-D-galactoside when the OD_{600} was ∼0.8. Addition of 0.2 mM ferrous ammonium sulfate to the growth cultures upon inoculation with preculture, upon induction, and 3 h after induction resulted in improved yields of the recombinant enzyme. The TPH fusion proteins were purified as previously described for a truncated form of TH (*19*). The fusion protein was cleaved by enterokinase (EK-Max from Invitrogen) (1 unit/0.04 μmol of fusion protein) in 50 mM Tris-HCl (pH 8.0), 1 mM $CaCl_2$, and 0.1% Tween 20 at 4 °C for 24 h. The isolated Δ90TPH proteins were separated from the fusion partner and the protease by size exclusion chromatography on a HiLoad Superdex 200 HR column (1.6 cm × 60 cm) (*20*).

Wild-type human PAH and PAH-W326F were expressed in *E. coli* (TB1 cells) as fusion proteins with maltose-binding protein and purified as described previously (*20*, *21*). The tetrameric forms of PAH and PAH-W326F were separated from aggregated forms and from maltose-binding protein and factor Xa by size exclusion chromatography (*22*). Protein concentrations were estimated spectrophotometrically using absorption coefficients A_{280} (1 mg mL^{-1} cm^{-1}) of 1.0 for wild-type human PAH (*20*) and 0.85 for PAH-W326F (*21*).

Assay of Tryptophan Hydroxylase and Phenylalanine Hydroxylase Activity. TPH activity was assayed at 30 °C in a standard reaction mixture (100 μL final volume) containing 40 mM Na-Hepes (pH 7.0), 0.05 mg/mL catalase, 10 μM ferrous ammonium sulfate, 2.5 mM dithiothreitol (DTT), 50 μM L-Trp (Sigma), and 250 μM (6*R*)-L-*erythro*-5,6,7,8-tetrahydrobiopterin (BH_4) (from B. Shircks). Iron was added first and the mixture allowed to preincubate for 3 min, and TPH was then added to the mixture, which was incubated with Fe(II) for an additional 5 min. The reaction started upon addition of BH_4 in DTT, and after a reaction period of 3 min, it was stopped by adding 100 μL of an acetic acid/ethanol mixture (pH 4.0) and placing the reaction mixture on ice. After centrifugation (10 min at 4 °C), the amount of 5-OH-Trp was measured in the supernatant by HPLC with fluorimetric detection (*23*). The amount of product was linear with time and the amount of enzyme added under the selected standard assay conditions. Steady-state kinetic studies of TPH inhibition by BH_2 (B. Schircks) were performed under standard conditions with 50 μM L-Trp, a variable concentration of BH_4 (from 0 to 500 μM), and in the absence or presence of BH_2 (200 and 400 μM). PAH activity was assayed as described previously (*20*). The kinetic parameters were calculated by nonlinear regression curve fitting.

Determination of the Iron Content. The amount of iron-bound holoenzyme in Δ90TPH was determined by extracting the iron from the purified enzyme by a modification of the method of Gottschall et al. (*24*) but using 10 mM bathophenanthroline disulfonate (Sigma) instead of *o*-phenanthroline, 1 mM L-Trp, 0.5 mM BH_4, and 1 mM DTT. The concentration of the released iron was calculated from the

molar extinction coefficient for the iron−bathophenanthroline complex at 535 nm (ϵ_{535} = 22 140 M^{-1} s^{-1}) (*25*).

Preparation of Samples for NMR, Data Collection, and Data Processing. Δ90TPH (~50 mg/mL) was prepared in 20 mM potassium phosphate and 0.2 M KCl (pH 7.2) containing 10% D_2O. BH_2 and L-Trp at the indicated concentrations were prepared together or in separated samples in the same 10% deuterated buffer. Experiments were performed on a Bruker DRX 600 MHz spectrometer equipped with pulse-field-gradient accessories at 291 K, except where otherwise indicated. In experiments with a variable field, measurements at 200 and 400 MHz were performed on Bruker AC-200 and Bruker DMX-400 spectrometers, respectively. The resonance assignments were made from $^1H-^{13}C$ HSQC and HMBC correlation experiments.

The longitudinal relaxation rates ($1/T_1$) were measured by the nonselective inversion recovery method (14 delays, 4 transients in each spectrum, 32K data points, 7184 Hz spectral width) in samples (0.5 mL) containing initially L-Trp and/or BH_2 (5 mM each) which were titrated with Fe(III)-bound Δ90TPH up to a final subunit concentration of 0.14 mM. The paramagnetic effects of enzyme-bound Fe(III) ($S = {}^5/_2$) on the longitudinal relaxation rates ($1/T_{1P}$) of the protons of bound L-Trp and BH_2 were measured using Δ90TPH preparations with known Fe(III) content. Iron−proton ligand distances were estimated using the normalized paramagnetic relaxation rates ($1/fT_{1P}$) by the Solomon−Bloembergen equations. The fraction of bound ligand forming the paramagnetic complex (*f*) was calculated as described previously (*15*, *26*) using the K_m(L-Trp) and the $K_i(BH_2)$ obtained in the kinetic characterization of Δ90TPH, and the amount of Fe(III) bound at the active site in each preparation. The absence of extraneously bound Fe(III) was confirmed by EPR spectroscopy (V. Schünemann, unpublished results). The effective correlation time (τ_c) for the electron−nuclear dipolar interaction in the TPH−Fe(III)·BH_2·L-Trp complex [defined as $\tau_c^{-1} = \tau_s^{-1} + \tau_M^{-1} + \tau_R^{-1}$, where τ_s is the electron-spin relaxation time, τ_M is the lifetime of the ligand protons in the bound state of the paramagnetic complex (exchange lifetime), and τ_R is the rotational correlation time of the paramagnetic complex] was calculated from the frequency dependence of the T_{1p} of several ligand protons, assuming that τ_c is frequency-independent and $\omega_I^2\tau_c^2 \gg 1$ (*27*). The outer sphere contribution to $1/T_1$, due to ligand nuclei binding at unspecific sites, was calculated by titrating a solution of 5 mM L-Trp, 6.3 mM BH_2, and 0.14 mM Δ90TPH with concentrated solutions (50−100 mM) of either β-2-thienylalanine, dopamine, noradrenaline, or L-Phe.

Transferred NOESY (TNOESY) spectra were collected at mixing times of 15, 30, 45, 60, and 75 ms in samples containing 5 mM L-Trp, 6.3 mM BH_2, and 0.14 mM enzyme subunit. Acquisition parameters included a 2 s relaxation delay, a 0.29 s acquisition time, a 7184 Hz spectral width, and 64 transients per t_1 increment. Raw data sets contained 200 and 2048 complex time domain data points in the t_1 and t_2 dimensions, respectively. Water suppression was achieved by using the "W5" pulse train (*28*) and excitation exculpting (*29*). Radiation damping effects were suppressed by a flip-back pulse (*30*) and bipolar pulse field gradient pairs (*31*). Data were processed with a complex linear prediction in F1 (2 × the number of time domain points in F1), a squared sine bell window function in both F1 and F2, and zero filling along F1 obtaining matrixes of 2048 × 2048 real data points. Interproton distances were estimated from the initial slopes of plots of the cross-peak volume as a function of mixing time (*32*−*34*), using distances of 2.47 and 2.60 Å between the H4 and H5 protons of L-Trp and the H8 and H7 protons of BH_2, respectively, as internal references.

Distance Geometry Calculations and Docking. Thirty structures of enzyme-bound conformers were generated from metal−proton, NOE distance restraints and chirality constraints using NMR Refine DGII (Insight II 2000, Accelrys) as described for BH_2 and L-Phe bound to PAH (*15*). The DOCK 4.0.1 suite of programs (University of California, San Francisco, CA) (*35*) was used to fit the bound conformers obtained from DGII into the modeled structure of TPH. The docking procedure and parameters were as described previously (*15*, *16*). In agreement with the distances between the metal and the ligand protons estimated by ^1H NMR, a GRID region with a 20 Å diameter surrounding the active site iron was defined for the docking procedure. Final optimization of the structure of the complexes was performed using Discover (Accelrys). The programs InsightII (Accelrys) and WebLab Viewer (Accelrys) were used to prepare the figures.

RESULTS

Molecular and Kinetic Characterization of Δ90TPH. The fusion protein of the wild-type form of recombinant human full-length TPH and its truncated form (Δ90TPH) were purified to homogeneity by affinity chromatography on a nickel-charged Chelating Sepharose Fast Flow gel, with a typical yield of ca. 25 mg of fusion proteins per liter of bacterial culture. When analyzed by size exclusion chromatography, the full-length form was found to be composed mainly of high-molecular weight inactive aggregated forms, while the deletion mutant Δ90TPH consisted mostly of soluble tetrameric forms, both as a fusion protein and as an isolated hydroxylase (40 kDa subunit). Moreover, this form was found to be stable and adequate for the planned NMR experiments; i.e., approximately 90% activity remained after incubation for 24 h at room temperature.

Both the native and truncated forms of TPH have been shown to require Fe(II) for activity (*12*, *36*, *37*). Using our standard assay conditions, the activity of purified TPHΔ90 was maximally increased 6.4-fold by preincubation of the enzyme with ferrous iron (data not shown). The concentration of Fe(II) required for half-maximal activation of the purified enzyme was 1.30 ± 0.58 μM, indicating a high affinity of the enzyme for the metal. These results also indicate that only a low proportion of the purified enzyme preparation contains iron. This was verified by assessing the formation of the Fe(II)−bathophenanthroline complex at 535 nm, obtaining a maximal amount of ~0.1 atom of iron/mol of subunit extracted after addition of 0.1 mM BH_4 and 1 mM DTT, and incubation at 50 °C for 1 h with the chelator (reducing conditions). After iron extraction, the resulting apoenzyme was devoid of catalytic activity in the absence of iron addition. The stoichiometry of the iron content in enzyme preparations has also been determined by EPR spectroscopy, and this technique has also shown that in the absence of BH_4 or reducing conditions the iron in Δ90TPH is present as Fe(III) ($S = {}^5/_2$) (unpublished results).

Table 1: Steady-State Kinetic Parameters for the Hydroxylation of L-Phe and L-Trp by Δ90TPH, Δ90TPH-F313W, PAH, and PAH-W326F[a]

enzyme	varied substrate	V_{max} (nmol mg^{-1} min^{-1})	K_m (μM)	V_{max}/K_m (μM^{-1} min^{-1})	$[V_{max}/K_m$(L-Trp)$]/[V_{max}/K_m$(L-Phe)$]$
Δ90TPH	L-Trp	77 ± 5	33 ± 4.5	0.12	0.9
	L-Phe	132 ± 19	48 ± 12	0.14	
Δ90TPH-F313W	L-Trp	17 ± 1	75 ± 6	0.01	0.5
	L-Phe	22 ± 2	60 ± 10	0.02	
PAH	L-Trp	32 ± 1	7 ± 1	0.23	1.1
	L-Phe	461 ± 8[b]	120 ± 18[b]	0.20	
PAH-W326F	L-Trp	211 ± 14	6 ± 1	1.81	36.2
	L-Phe	355 ± 14[b]	367 ± 5[b]	0.05	

[a] The measurements were performed under standard assay conditions, including 10 mM ferrous ammonium sulfate and 250 μM BH_4. [b] Data from ref *21*.

Both native and recombinant TPH enzymes have been shown to hydroxylate both L-Trp and L-Phe, but not L-Tyr (*12*, *38*−*40*). Δ90TPH was also able to hydroxylate L-Trp and L-Phe, and the apparent steady-state kinetic constants for the hydroxylation of both amino acids with BH_4 are shown in Table 1. The apparent K_m value for BH_4 was 50.8 ± 16.0 μM. Moreover, Δ90TPH exhibited weak substrate inhibition by both L-Trp (>150 μM) and L-Phe (>100 μM). BH_2 has been shown to be a competitive inhibitor of BH_4 for both human recombinant TH (*26*), rat PAH (*14*, *41*), and human PAH (*15*) with K_I values of ∼70, 50−60, and 100 μM, respectively. To our knowledge, no previous study has been reported on the inhibitory effect of BH_2 on TPH activity. Steady-state kinetic analyses showed that BH_2 is a nearly competitive inhibitor of Δ90TPH versus the natural cofactor BH_4 with a K_I value of 0.161 ± 0.03 mM.

Paramagnetic Contribution to the Relaxation Rates, Dipolar Correlation Time, and Iron−*Proton Distances.* The ^{1}H NMR spectrum of L-Trp and BH_2 is shown in Figure 1A. Complete resolution was achieved at 600 MHz. The addition of the holoenzyme [Fe(III)−ΔTPH] resulted in typical paramagnetic effects, which were observed as line broadening (data not shown) and as an increase in the $1/T_1$ of the protons (shown in Figure 1B for the aromatic protons of L-Trp). Interestingly, the largest paramagnetic effect was observed for the H5 proton of L-Trp, which is the site of hydroxylation (Figure 1B). The closest of the stable protons in BH_2 was H1′ of the dihydroxypropyl side chain, indicating a different conformation of TPH-bound BH_2 with respect to that of PAH-bound BH_2, in which case the closest proton to the active site iron was H7 (*15*). Several compounds were tested as competitive ligands to displace the substrate and the cofactor analogue from the ternary TPH−Fe(III)·BH_2·L-Trp complex and to calculate the outer sphere contribution to $1/T_{1P}$. Neither dopamine nor noradrenaline had any effect on the $1/T_{1P}$ of either L-Trp or BH_2 when tested at concentrations up to 6 mM. In contrast, L-Phe and β-2-thienylalanine were effective in displacing L-Trp from the ternary complex in a concentration-dependent manner, and β-2-thienylalanine, but not L-Phe, also displaced BH_2 (data not shown). A zero outer sphere effect was estimated for both L-Trp and BH_2 at 18 mM β-2-thienylalanine. The normalized paramagnetic relaxation rates ($1/fT_{1P}$) (*42*) are shown in Table 2.

The effective dipolar correlation time (τ_c) for the Δ90TPH−Fe(III)·BH_2·L-Trp complex was calculated to be (1.19 ± 0.36) × 10^{-10} s from the field dependency of T_{1P} for various aromatic and aliphatic protons of L-Trp and BH_2 (Figure 2

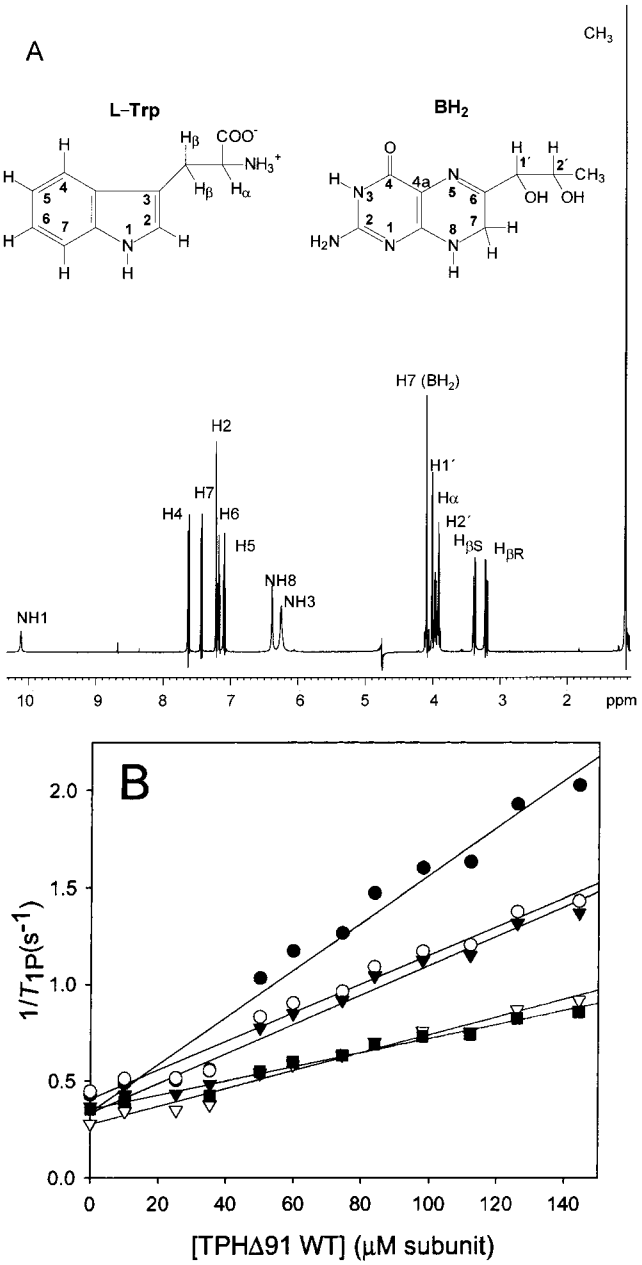

FIGURE 1: (A) One-dimensional ^{1}H NMR spectrum (128 transients) of L-Trp (5 mM) and L-*erythro*-7,8-dihydrobiopterin (BH_2) (6.2 mM), with assignments, collected at pH 7.2, 10% deuterium oxide, and 291 K, in the presence of 0.14 mM subunit Δ90TPH. (B) Paramagnetic effects of hTPHΔ90 on the aromatic protons of L-Trp (5 mM). Paramagnetic relaxation rates ($1/T_{1P}$) were measured vs enzyme concentration for the H5 (●), H4 (○), H6 (▼), H7 (▽), and H2 (■) protons.

Table 2: Normalized Paramagnetic Relaxation Rate $1/fT_{1P}$ (s^{-1}) and Distances (r) from the Observable Protons of Bound L-Trp and BH_2 to the Fe(III) in Δ90TPH and Comparison with Distances Obtained after Docking

	nucleus	δ (ppm)	$1/fT_{1P}$ ($\times 10^{-1}$ s^{-1})	r (Å)[a]	r (Å)[b]
L-Trp	H4	7.625	148.6 ± 6	6.2 ± 1	4.7−6.4
	H7	7.432	92.1 ± 3	6.7 ± 1	5.7−6.4
	H2	7.215	72.9 ± 2	7.0 ± 1	7.8−9.6
	H6	7.175	152.4 ± 2	6.2 ± 1	3.9−4.9
	H5	7.091	244.9 ± 8	5.7 ± 1	3.8−4.4
	Hα	4.008	54.7 ± 7	7.3 ± 1	6.5−7.9
	pro-S Hβ	3.381	42.6 ± 9	7.6 ± 2	6.7−9.4
	pro-R Hβ	3.250	42.5 ± 8	7.6 ± 2	8.0−9.9
BH_2	H7[c]	4.087	26.0 ± 2	8.0 ± 2	7.7−8.1
	H1′	4.008	44.8 ± 4	7.6 ± 2	6.7−8.0
	H2′	3.912	28.2 ± 4	7.9 ± 2	8.8−9.1
	CH_3[c]	1.125	26.0 ± 3	8.0 ± 2	7.6−8.8

[a] Estimated from the paramagnetic probe T_1 method. Total errors in the absolute distances (r) include contributions of errors in $1/fT_{1P}$ and τ_c. Errors arising from τ_c would affect all distances equally so that the errors in the relative values are <10%. Thus, the relative values are most meaningful despite the apparent imprecision in the absolute distances. [b] Iron−proton distances measured after docking. [c] Average position of these protons.

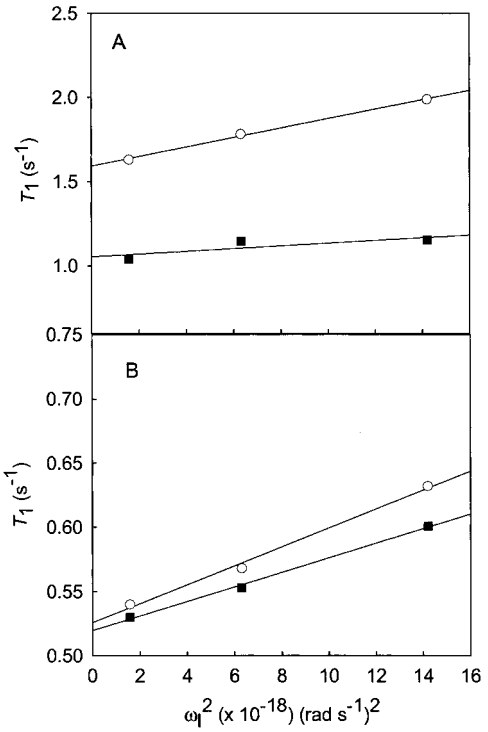

FIGURE 2: Effect of magnetic field on the paramagnetic relaxation time (T_{1P}) for (A) the H7 protons of L-Trp and (B) the methyl (CH_3) protons of BH_2. Measurements were performed at 291 K with 40 (○) and 89 (■) μM TPHΔ90 subunit, 5 mM L-Trp, and 6.3 mM BH_2. ω_I is the Larmor precession frequency. A τ_c value of (1.19 ± 0.36) × 10^{-10} s was estimated.

and data not shown). This value should be considered as an approximation since it was calculated from measurements at high fields (≥100 MHz), where dispersion of magnetization may occur (*43*). The value of τ_c is determined by the fastest of the individual components (τ_s, τ_M, and τ_R). τ_R is estimated from the Stokes law for the rotation of a rigid sphere in a viscous medium to be ≈2.7 × 10^{-13} times the relative molecular mass (*42*), giving a value of ≈1.1 × 10^{-8} s for Δ90TPH, while τ_M has been shown to be ≥10^{-9} s (*42*, *44*). Thus, the dipolar correlation time appears to be dominated by τ_S, the electron-spin relaxation time for high-spin Fe(III) (*42*, *45*). Moreover, from the effect of the temperature (18−40 °C) on the $1/T_{1P}$, we calculated Arrhenius activation energies (E_a) of 3.7 and −16 kJ/mol for the paramagnetic contribution to the relaxation of bound BH_2 and L-Trp, respectively. In general, τ_M has E_a values of ≥9 kJ/mol, and the typical E_a values for $1/T_{1P}$ in exchange-limited processes are ≥13 kJ/mol (for reviews, see refs *27* and *44*). Thus, the large differences in the $1/fT_{1P}$ values (Table 2), the frequency dependency, the low E_a value, and the fact that $1/fT_{2P}$ values are ca. 8- and 7-fold greater than the $1/fT_{1P}$ values (data not shown) all indicate that fast exchange exists for the ligands in the TPH−Fe(III)·BH_2·L-Trp complex and that the Fe(III)−proton distances can be estimated from the $1/fT_{1P}$ values (Table 2).

Transferred NOESY (TNOESY) Spectra. TNOESY spectra of L-Trp and BH_2 in the presence of Δ90TPH present positive cross-peaks, reflecting negative NOEs, typical of ligands bound to the enzyme (Figure 3). The corresponding cross-peaks in the NOESY spectra (1 s mixing time, data not shown) collected in the absence of the enzyme were negative, thus confirming that a transfer NOE is being observed. No intermolecular cross-peaks between protons of BH_2 and L-Trp were observed. For L-Trp, positive cross-peaks were observed between the aromatic protons, between the aromatic H2 and H4 and the aliphatic Hα and Hβ protons, and between the aliphatic protons (Figure 3B). Comparison of the NOESY spectra of L-Trp taken in the absence and presence (TNOESY) of TPH shows that the L-Trp cross-peaks in the NOESY spectra are also observed in the TNOESY spectra and have similar intensity but positive. That indicates that the conformation of bound L-Trp resembles that of the amino acid free in solution at neutral pH; i.e., there are no large binding-induced changes in the conformation of the substrate. On the other hand, and similar to what was found for the BH_2−PAH complex, strong cross-relaxation is found between H1′ and H2′ of the dihydroxypropyl side chain at C6 in TPH-bound BH_2 (Figure 3B) that is not found in the enzyme free samples (*15*). No cross-peak appeared between either H7 or H1′ and the methyl protons of BH_2, which is different from the case for the PAH−BH_2 complex. The approximate interproton distances calculated from the TNOESY data are summarized in Table 3.

Distance Geometry Calculations. Thirty sets of molecular coordinates were computed by DGII in the embedding step of the calculation and refined as described previously (*46*). A few conformers violated the criteria established by the relative iron−proton distances (Table 2). The ensemble of remaining conformers of L-Trp (three families) and BH_2 (three families) (Figure 4) showed pairwise root-mean-square deviation (rmsd) values for all atoms of 0.65 and 0.90 Å, respectively. Apart from a few exceptions where the interproton distances seem to be underestimated by the TNOESY measurements, there is good agreement between the intramolecular distances measured in the final bound conformers and the estimated distances used as restraints (Table 3). Opposite to that which is found in the TH−BH_2 (*47*) and PAH−BH_2 (*15*) complexes, where the dihydroxypropyl chain at C6 bends toward the pyrazine ring, in TPH-bound BH_2 the configuration of the side chain is more extended, with N5−C6−C1′−C2′ and C6−C1′−C2′−C3′ torsion angles of 122 ± 7° and −61 ± 3°, respectively. This is in agreement

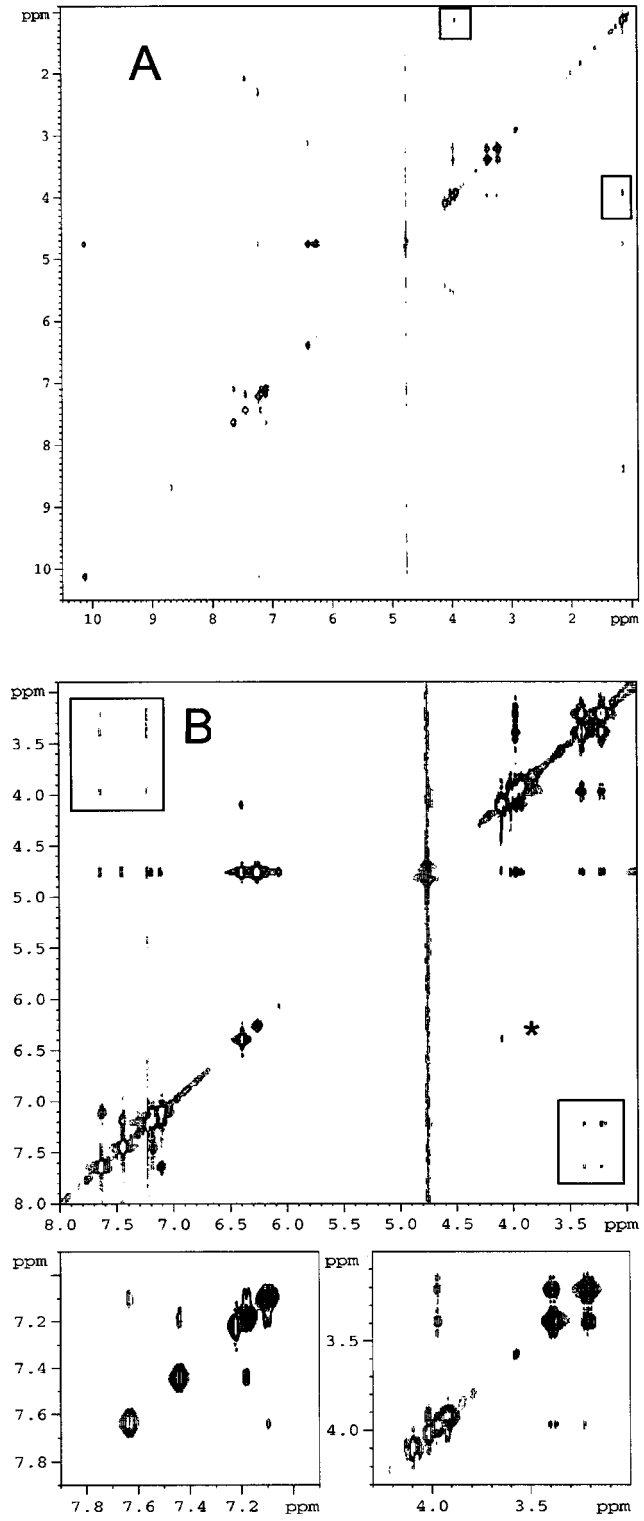

FIGURE 3: Transferred NOESY (TNOESY) spectrum of L-Trp and BH_2 in the presence of enzyme. Conditions: 5 mM L-Trp, 6.3 mM BH_2, 0.14 mM TPHΔ90, pH 7.2, 10% deuterium oxide, 291 K, and a mixing time of 75 ms. (A) Complete spectrum. The CH_3 protons only show interaction with the H2′ proton (inside box). (B) Extended contour plots showing different regions of the TNOESY spectrum. The cross-peaks between the H4 and H2 aromatic protons and the aliphatic protons of L-Trp (inside box), between the H7 and H8 protons of BH_2 used as an internal standard (*), between the aromatic (bottom left) and aliphatic (bottom right) protons of L-Trp, and between the H1′ protons and the H2′ and H7 protons of BH_2 (bottom right) are shown.

with the lack of cross-peaks between the resonance of the CH_3 protons with either the H7 protons or the H1′ in the

Table 3: Intramolecular Proton−Proton Distances for L-Trp and BH_2 Bound to Δ90TPH

	proton pair	r (Å)[a]
L-Trp	H4−H5	2.47[b]
	H4−Hα	3.0 ± 0.2 (2.8)
	H4−*pro-S* Hβ	2.9 ± 0.3 (2.9)
	H4−*pro-R* Hβ	3.0 ± 0.3 (4.0)
	H2−Hα	3.8 ± 0.4 (4.6)
	H2−*pro-S* Hβ	2.9 ± 0.2 (3.6)
	H2−*pro-R* Hβ	2.6 ± 0.2 (2.7)
	Hα−*pro-S* Hβ	2.4 ± 0.4 (2.3)
	Hα−*pro-R* Hβ	3.0 ± 0.8 (3.1)
BH_2	H8−H7[c]	2.6[b]
	H7[c]−H1′	2.6 ± 0.4 (2.9)
	H1′−H2′	2.4 ± 0.2 (2.4)

[a] Distances estimated from TNOESY spectra and, in parentheses, distances measured after distance geometry calculations (in the structure with the lowest rmsd). [b] Internal standard. [c] Degenerate protons.

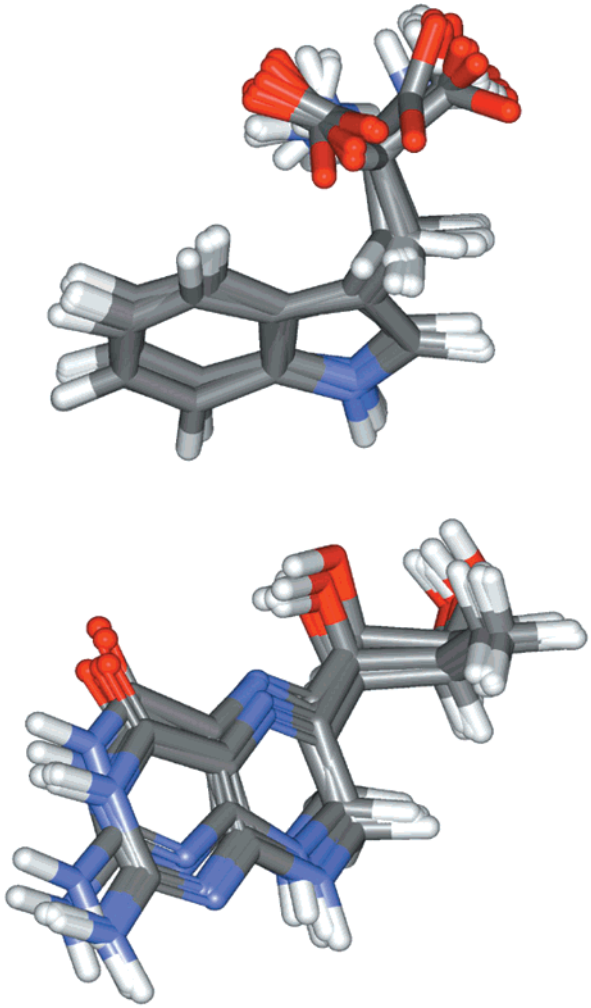

FIGURE 4: Superimposed distance geometry-refined structures of L-Trp (top) and BH_2 (bottom) bound at the active site of hTPHΔ90 based on the experimental NMR distances given in Tables 1 and 2.

TNOESY spectrum (Figure 3). Moreover, the conformers of BH_2 exhibited an almost-*cis* configuration of the hydroxyls around the C1′−C2′ bond (Θ, OH−C1′−C2′−OH = −57 ± 2°), in agreement with the strong cross-relaxation between the H1′ and H2′ protons (Figure 3).

Modeled Structure of TPH and Molecular Docking. No successful crystallization of TPH or its truncated forms has

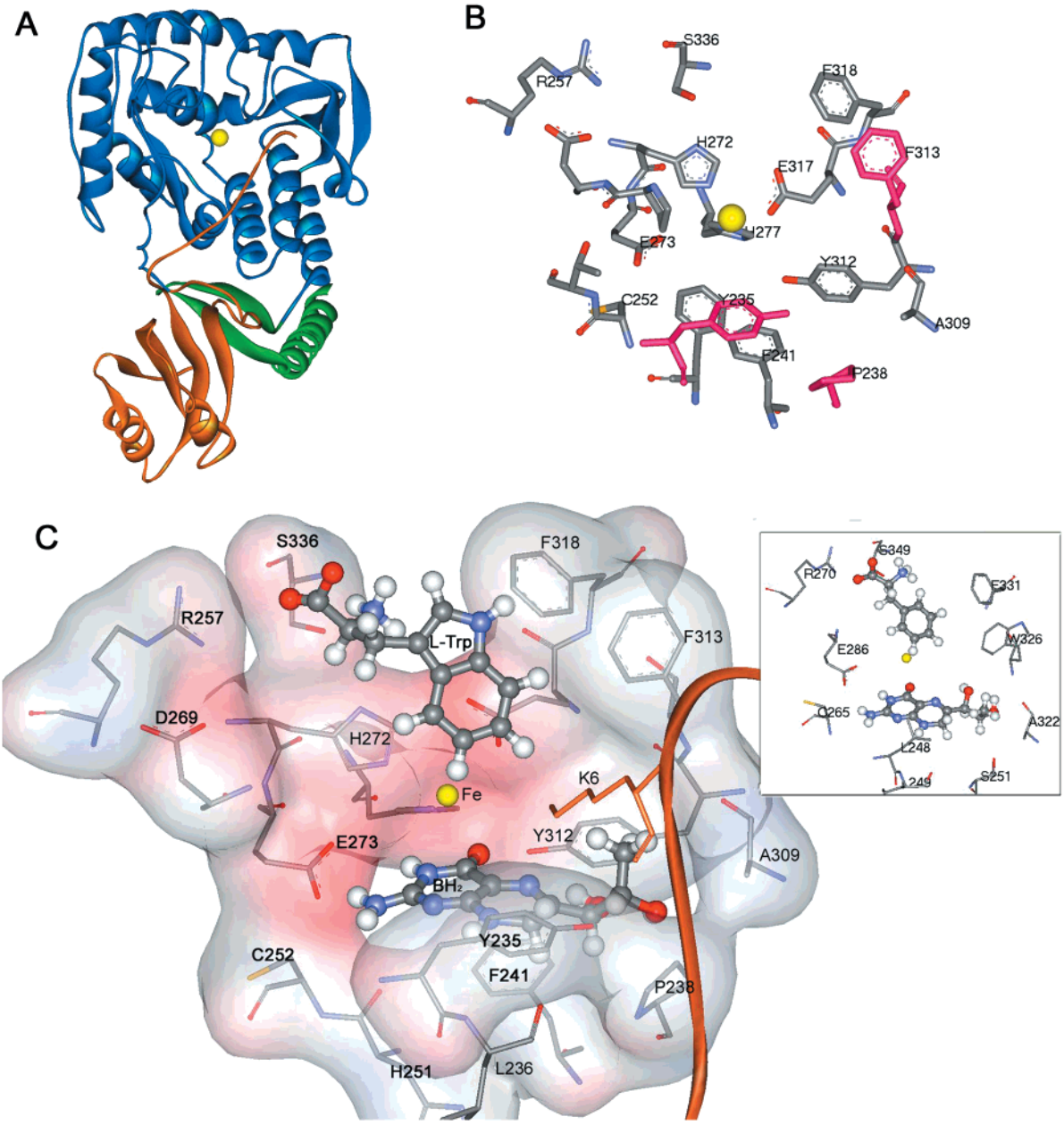

FIGURE 5: Modeled structure of TPH and molecular docking of L-Trp and BH_2 into the enzyme. (A) Overall structure of the full-length subunit of human TPH showing the regulatory (orange), catalytic (blue), and oligomerization (green) domains. The iron atom is shown in yellow. (B) Detailed structure of the active site region. Residues of human TPH not conserved in the aromatic amino acid hydroxylases are shown in pink. (C) Docked structure of L-Trp and BH_2. Active site residues at the ligand binding sites are shown as sticks, and L-Trp and BH_2 are shown in ball-and-stick representations (nitrogen in blue, oxygen in red, and carbon in gray). The N-terminal sequence is shown in orange. The iron is shown in yellow. Docking by DOCK 4.0 was performed in vacuum, using the solvent accessible area of the receptor and the structure with the lowest rmsd relative to the ensembles in Figure 4. The inset shows the PAH·BH_2·L-Phe complex according to Teigen et al. (*15*).

been reported yet, despite intensive efforts by several research groups. However, the high level of sequence identity between the three mammalian hydroxylases, notably, at the catalytic domains, allows the preparation of structural models for TPH by sequence alignment modeling (*3*, *18*). Figure 5A shows the structural model of TPH prepared using phosphorylated full-length PAH (PDB entry 1PHZ) refined to 2.2 Å resolution (*7*) as a template using the Homology module of InsightII 2000 (Accelrys) (*3*). The catalytic domain of TPH has a similar basketlike arrangement of α-helices and *β*-strands and loops as in PAH and TH with the active site consisting of a 13 Å deep and 10 Å wide pocket where the non-heme iron is placed by coordination to the conserved His272, His277, and Glu317 residues (Figure 5). Interestingly, while most of the residues at the active site seem to be conserved among the aromatic amino acid hydroxylases, there are a number of nonconserved residues which may be involved in substrate specificity or in differential binding for BH_2 (i.e., Phe313, Tyr235, and Pro238) (Figure 5B).

The enzyme-bound conformers of L-Trp and BH_2 generated by NMR-based DGII were docked into the modeled structure of human TPH using DOCK 4.0 (*35*). Lowest energy scores were obtained for docked configurations generated from the structures of L-Trp and BH_2 with the

lowest rmsd relative to the ensemble of "enzyme-bound" DGII-generated conformers. The top-scoring docked conformers are shown in Figure 5C. Similar structures were obtained when the flexibility of the ligands was allowed during docking, an indication of the validity of the NMR-based structures. Of the 30 conformers docked into the TPH model, all configurations of the ligands were located at their expected binding site by analogy with the PAH−BH_2 complex (*15*, *17*). As seen in Table 2, the distances from the active site iron to the observable protons of the docked conformers of L-Trp and BH_2 correlate well with the relative distance estimates from the paramagnetic probe T_1 measurements. The largest differences in the absolute Fe(III)−proton distances are those for the most closely located protons, i.e., H5 and H6 of L-Trp (Table 2). These distances may have been overestimated by the NMR method because L-Trp could not be docked into the modeled structure of TPH when the distance between either H5 or H6 and the Fe(III) is set to an absolute value of 6 Å (data not shown).

In the docked structure, L-Trp forms hydrogen bonds with Arg257 and Ser336, and the indole side chain π-stacks with His272 and is close to Phe318 and Phe313. The pterin ring of BH_2 π-stacks with Phe241, and N3 and the amine at C2 hydrogen bond with the carboxylic group of Glu273. The ring also establishes specific contacts with His251. The distance between the O4 atom of BH_2 and the iron (2.7 ± 0.2 Å) is compatible with coordination, as previously found for the PAH−BH_2 complex. The OH2′ in the side chain at C6 is placed within hydrogen bonding distance of the carbonyl group of Ala322.

Significance of Phe313 (TPH) and Trp326 (PAH) in Substrate Specificity: Mutagenesis Studies. The BH_2 binding site found by NMR/molecular docking in TPH corresponds to the pterin site in PAH as determined by NMR/docking (*15*) and by crystallography (*17*), although some differences in the detailed interactions between the pterin and the enzyme are encountered by the two methods. On the other hand, no crystal structure is yet available for complexes of the aromatic amino acid hydroxylases with their amino acid substrates. The participation of the conserved Arg257 (TPH) in substrate binding has been supported by site-directed mutagenesis studies with TH (*48*), while mutations at the conserved Ser336 (TPH) result in an aggregating protein (*49*, *50*), uncoupled reactions (*51*), and a reduced affinity for the substrate (*52*). As seen in Figure 5C, another important residue in the substrate binding site is Phe313, which, interestingly, is not conserved among the hydroxylases (Figure 5B); i.e., it is a Trp in both TH and PAH. Thus, the role of this residue in determining the extent of substrate binding and substrate specificity was investigated by site-directed mutagenesis and kinetic studies. The mutant Δ90TPH-F313W was expressed and purified by the same procedures as described for Δ90TPH (see Experimental Procedures), and its kinetic parameters were measured with both L-Trp and L-Phe as substrates (Table 1). PAH and its mutant PAH-W326F (*21*) were also examined for their ability to hydroxylate L-Trp. The characteristic positive cooperativity for L-Phe binding is also manifested by both PAH and PAH-W326F with L-Trp as the substrate (Hill coefficient = 1.9) (Figure 6). Also, as shown in Table 1, the relative preference of L-Phe and L-Trp as substrates is switched when this amino acid is subject to a "conservative" replacement. In PAH, the W326F mutation creates an enzyme with a relative preference for L-Trp, while the preference for L-Trp decreases when the reverse mutation (F313W) is introduced into TPH.

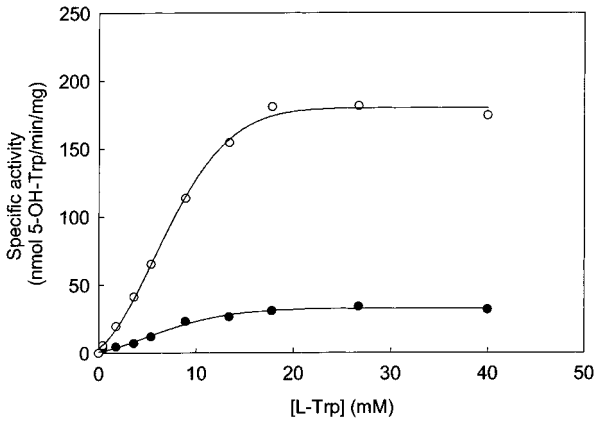

FIGURE 6: Initial rate of tryptophan hydroxylation as a function of L-Trp concentration with 2 μM subunit PAH (wild type) (●) and PAH-W326F (○).

DISCUSSION

Kinetic and Molecular Characterization of Δ90TPH. It is known that full-length TPH is unstable and difficult to purify (*8*, *9*). However, the truncated form Δ90TPH is a soluble, stable, and active form of TPH, which has allowed its study by NMR. Δ90TPH was found to be a tetramer, as expected, since as seen in the modeled 3D structure of TPH (Figure 5A) this form retains the long C-terminal α-helix, which by homology with TH and PAH, is essential for tetramer formation through domain swapping interactions among subunits (*4*, *6*). However, it has also been reported that dimeric and monomeric forms of the enzyme can result from N-terminal truncations (*53*).

The kinetic properties of TPH from different sources have been studied using a variety of assay conditions and pterin cofactor analogues, complicating a direct comparison (*9*). Nevertheless, the K_m values obtained in this study for Δ90TPH fall within the range of reported values for recombinant TPH from different sources, i.e., K_m values for L-Trp, L-Phe, and BH_4 of 12−48 μM (*12*, *36*, *40*), 61 μM (*12*), and 28−135 μM (*12*, *36*, *40*), respectively. While the K_m values do not seem to be significantly affected by the N-terminal truncation, the maximal activity of TPH is decreased in the absence of the N-terminal region (*9*). Thus, full-length human TPH, isolated as a fusion protein with maltose-binding protein, exhibits a V_{max} of 240 ± 9 nmol min^{-1} mg^{-1} with L-Trp as the substrate (Ekern et al., unpublished results), i.e., ∼3-fold higher than the activity of Δ90TPH or similar truncated forms of TPH. The decreased activity of TPH in the absence of the N-terminal region is characteristic of this enzyme, and is the opposite of the findings for PAH and TH, for which it has been shown that the N-terminal sequence exerts a negative control over the catalytic activity (*1*, *22*). The most significant effect of the N-terminal truncation on TPH is the increase in stability that is achieved, allowing large-scale purification and physicochemical characterization of the truncated forms, as has been the case in this work for Δ90TPH. The molecular basis for the inherent instability associated with the presence of

the N-terminus is not known, but seems to be specific for TPH, since it is not observed for the isolated forms of TH or PAH.

The immediate BH_4 oxidation product generated in the TPH reaction is a 4a-hydroxytetrahydrobiopterin (*10*, *12*), which is rapidly converted into (6*R*)-quinonoid dihydrobiopterin. The latter compound subsequently isomerizes to 7,8-dihydrobiopterin (BH_2). At neutral pH and 20−23 °C, both 4a-hydroxytetrahydrobiopterin and (6*R*)-quinonoid dihydrobiopterin are quite unstable, with $t_{1/2}$ values of 0.75−1.2 (*54*) and 0.6 min (*55*), respectively. Thus, these compounds were considered to be unsuitable for the lengthy NMR studies performed here. On the other hand, BH_2 is stable, and as found previously for the other two aromatic amino acid hydroxylases (*2*, *15*, *26*), it is a competitive inhibitor versus the natural cofactor BH_4 ($K_i \approx 0.16$ mM). BH_2 was therefore considered to be an appropriate structural analogue of BH_4.

Paramagnetic Iron in TPH. Although only indirect evidence for the iron requirement of TPH is available from enzyme kinetic experiments, it is widely accepted by analogy with TH and PAH that TPH is also an iron-containing metalloenzyme (*12*, *56*, *57*). Accordingly, Δ90TPH has an absolute requirement for Fe(II) for activity. As previously found for recombinant human TH (*58*), Δ90TPH contains as isolated a substoichiometric amount of iron per subunit and is activated by incubation with Fe(II) salts which bind with high affinity (concentration of iron at half-maximal activation = 1.3 ± 0.5 μM). As seen by NMR, in the absence of reducing conditions or BH_4, the iron incorporated at the active site of Δ90TPH, as isolated, has a large paramagnetic effect on the ligand protons, characteristic of the oxidized ferric form. Also, the electron-spin relaxation time (τ_s) calculated for the first time in the present study ($\approx 1.1 \times 10^{-8}$ s) is typical for high-spin Fe(III) (*42*, *45*).

The highest paramagnetic contribution of the iron to the relaxation and the shortest iron−proton distance were obtained for H5 of L-Trp, which is the site of hydroxylation. This result is important in assigning a key role to the iron in the hydroxylation reaction by TPH and is in agreement with recent mechanistic data supporting the idea that the direction of the NIH shift occurring upon hydroxylation of L-Trp is from C5 to C4 (*59*). The displacement experiments also provide insight into the competitiveness of the binding of substrate analogues and inhibitors. Neither dopamine nor noradrenaline (≤6 mM) was able to displace L-Trp or BH_2. Catecholamines have been shown to competitively inhibit PAH and TH with respect to the pterin cofactor and displace BH_2 from its binding site in human TH (*47*) but not in human PAH (*15*). There are several reports that compounds having a catechol structure markedly inhibit TPH with a noncompetitive inhibition versus both L-Trp and BH_4 (*60*, *61*); i.e., the catechol structure seems to combine with TPH at a binding site kinetically different from that of the substrate or cofactor. Thus, our binding results seem to concur with the enzyme kinetic experiments showing a noncompetitive inhibitory nature of catecholamines.

Conformation of L-Trp and BH_2 Bound to TPH. As inferred from the docking results (Figure 5C), the residues involved in L-Trp binding to TPH are mainly (i) Arg257, which establishes an ionic interaction with the carboxyl group of the amino acid substrate, (ii) Ser336, which hydrogen bonds with the amino group, and (iii) His272, Phe313, and Phe318, which interact with the aromatic ring through stacking interactions. The stacking of the aromatic ring with the iron-coordinating His272 may be important for a correct positioning of the H5 proton toward the metal. Except for Phe313 (see below), these substrate-binding residues are conserved in the aromatic amino acid hydroxylases and have also been found to be involved in the interaction of L-Phe with PAH (*15*). On the basis of the increased K_m for L-Trp shown by the Y235A and Y235L mutants, Jiang et al. (*18*) have recently reported that Tyr235 is positioned at the L-Trp binding site in TPH. However, according to our results and recent X-ray crystallography studies (*17*), this residue is located at the pterin binding site. In fact, the Y235A and Y235L mutants also exhibit decreased $K_m(BH_4)$ values (*18*) which can in turn affect the apparent affinity for L-Trp. Both Tyr235 and Pro238, which are nonconserved, are located at one side of the binding site of the dihydroxypropyl side chain (Figure 5) and appear to be responsible for a more restrictive binding site in TPH that results in a more extended configuration of this chain in TPH-bound BH_2 than in the pterin bound to the other hydroxylases. A reason for this appears to be that the bulky ring of Tyr235 comes very close to the dihydroxypropyl side chain of BH_2 (the OH in Tyr235 is 2.4 Å from the H1′ in BH_2) (Figure 5C), impeding a bending of the chain toward the pterin ring similar to that found for PAH-bound BH_2 (Figure 5C, inset). As a consequence, and in agreement with the lack of cross-relaxation between the CH_3 protons and either the H7 or H1′ proton, the distance between the methyl protons and H7 in the TPH-bound BH_2 conformers is ∼5.3 Å, while it was 3.9 Å for PAH-bound BH_2 (*15*). Both TH and PAH have a Leu at this position, and this residue does not interfere with the dihydroxypropyl side chain (*15*−*17*). Despite these differences in the conformation of BH_2 bound to the three hydroxylases, an almost-*cis* conformation was manifested for the two hydroxyl groups at C1′ and C2′ in TPH-bound BH_2 ($\Theta = -57°$) (Figure 4), similar to that which has been found for TH- and PAH-bound BH_2 (*15*, *17*, *47*). The configuration for the hydroxyls appears to be almost-*trans* ($\Theta = -160°$) in free BH_2 (*15*, *62*). Thus, a *trans* to *cis* conformational change occurs upon BH_2 binding to all three hydroxylases. It is interesting to note that the configuration of the hydroxyls is almost-*cis* for BH_4 at neutral pH free in solution (*62*), and it seems that the analogue BH_2 adopts the configuration of the natural cofactor upon binding to the hydroxylases. Both Tyr312 and Ala309 seem to be involved in determining the proper configuration of the side chain. While the Tyr residue is conserved among the aromatic amino acid hydroxylases, Ala309 corresponds to Ala322 in PAH and to Ser368 in TH [it is also Ala in quail TH (*63*)].

It seems clear that for TH and PAH the regulatory properties elicited by the natural cofactor BH_4 as a negative effector are associated with the presence of the dihydroxypropyl side chain at position 6*R*, and at least for PAH, the negative effects may be explained by specific interactions between this side chain and the N-terminal autoregulatory sequence (*17*). In BH_2 docked into TPH, the methyl group is also at contact distances from Lys6 at the N-terminal region that covers the entrance of the active site in the modeled structure of TPH (Figure 5A,C). Further kinetic and structural studies with TPH, including cofactor analogues, are necessary to understand the kinetic and regulatory

implications of the different configuration of the dihydroxypropyl side chain between the three aromatic amino acid hydroxylases. A range of synthetic pteridines have been prepared with the aim of modifying the biosynthesis of monoamines in the nervous system (*16*). Our finding of enzyme-specific interactions of BH_2 with the enzyme active sites implies that it may be possible to design BH_4 analogues which produce selective modulation of serotonergic (TPH) versus catecholaminergic (TH) neurotransmission.

As deduced from the docked structure, additional interactions of BH_2 with TPH also include an aromatic π-stacking of the pterin ring with the conserved Phe241 at the bottom of the wide active site crevice structure (Figure 5). Moreover, N3 and the amine group at C2 hydrogen bond with the carboxyl group of the conserved Glu273 and the distance between the O4 atom of BH_2 and the iron (2.7 ± 0.2 Å) is also compatible with coordination, in agreement with data obtained with the other hydroxylases by NMR and docking (*15*, *16*). In the crystal structure of the PAH−BH_2 complex, however, N3 and O4 of BH_2 interact with the corresponding Glu286 and the iron, respectively, through bridging with two iron-coordinating water molecules, resulting in the pterin ring being located at distances not compatible with coordination to the iron (*17*). The reasons for these discrepancies are not clear, although as recently discussed in a study of docking of BH_4 to TH (*16*), these coordinating water molecules seem to have an increased tendency to be removed by ligand binding since they have high temperature factors (*64*). Nevertheless, the structural studies on PAH show that the cofactor is in an ideal orientation and conformation for dioxygen to bind in a bridging position between the iron and the C4a atom of the pterin, forming a putative iron−4a-peroxytetrahydropteridine transient intermediate that would be either the hydroxylating species itself (*13*, *15*) or the precursor of a ferryl oxo intermediate (*51*). In the structure of the ternary TPH−Fe(III)·L-Trp·BH_2 complex, the amino acid and the pterin are also at adequate distances for the intercalation of iron-coordinated oxygen and for the formation of a transient iron−4a-peroxytetrahydropterin intermediate in the reaction; i.e., C5 of L-Trp and C4a of the pterin are located 4.1 ± 0.3 and 4.4 ± 0.3 Å from the iron, respectively, and 6.1 ± 0.4 Å from each other.

Significance of Phe313 and Trp326 in Substrate Specificity: Mutagenesis Studies. TPH and PAH probably originate from a common ancestral gene (*65*). Among the changes which have probably occurred from this gene is the W313/326F mutation. As seen in Figure 6, Phe313 of TPH seems to be involved in the binding of the indole ring of L-Trp and corresponds to a Trp in both TH and PAH. Thus, this residue was chosen as a candidate for site-directed mutagenesis studies intended to investigate the structural basis of substrate specificity. In the study presented here, the point mutation F313W was shown to effectively switch the apparent binding affinity of the amino acid substrates, L-Trp and L-Phe, for Δ90TPH. Opposite to the situation for Δ90TPH where the affinity for L-Trp is higher than that for L-Phe, the mutant F313W shows a higher preference for L-Phe than for the natural substrate L-Trp. On the other hand, the mutant W326F in PAH has a lower affinity for its natural substrate, L-Phe, than the wild-type form (Table 1). Thus, it appears that Phe313 of TPH and Trp326 of PAH are important residues in determining the substrate specificity of TPH and PAH. In fact, the W326F mutant of PAH may be considered a "super-TPH" in that its relative preference for L-Trp is even higher than in TPH. Earlier reports have claimed that a single gene encodes both tryptophan and phenylalanine hydroxylase activities in *Drosophila melanogaster* (*66*), and a Trp was located in this TPH or PAH gene at the position corresponding to Trp326 or Phe313, respectively. However, the recent elucidation of the genome sequence of *Drosophila* has shown the TPH activity is encoded by a gene separate from the PAH activity, and contains a conserved Phe at the relevant position (*67*). The mutation from the Trp residue in PAH to the Phe residue in TPH seems to be related to the need to accommodate the bulkier Trp at the active site with a consequent conservation of active site volume.

ACKNOWLEDGMENT

We thank Randi M. Svebak and Sidsel Riise for expert technical assistance.

REFERENCES

1. Kaufman, S. (1993) *Adv. Enzymol. Relat. Areas Mol. Biol. 67*, 77−264.
2. Kappock, T. J., and Caradonna, J. P. (1996) *Chem. Rev. 96*, 2659−2756.
3. Martínez, A., Knappskog, P., and Haavik, J. (2001) *Curr. Med. Chem. 8*, 1077−1092.
4. Goodwill, K. E., Sabatier, C., Marks, C., Raag, R., Fitzpatrick, P. F., and Stevens, R. C. (1997) *Nat. Struct. Biol. 4*, 578−585.
5. Erlandsen, H., Fusetti, F., Martínez, A., Hough, E., Flatmark, T., and Stevens, R. C. (1997) *Nat. Struct. Biol. 4*, 995−1000.
6. Fusetti, F., Erlandsen, H., Flatmark, T., and Stevens, R. C. (1998) *J. Biol. Chem. 273*, 16962−16967.
7. Kobe, B., Jennings, I. G., House, C. M., Michell, B. J., Goodwill, K. E., Santarsiero, B. D., Stevens, R. C., Cotton, R. G., and Kemp, B. E. (1999) *Nat. Struct. Biol. 6*, 442−448.
8. Cash, C. D. (1998) *Gen. Pharmacol. 30*, 569−574.
9. Mockus, S. M., and Vrana, K. E. (1998) *J. Mol. Neurosci. 10*, 163−179.
10. Kowlessur, D., and Kaufman, S. (1999) *Biochim. Biophys. Acta 1434*, 317−330.
11. Hamdan, F. F., and Ribeiro, P. (1999) *J. Biol. Chem. 274*, 21746−21754.
12. Moran, G. R., Daubner, S. C., and Fitzpatrick, P. F. (1998) *J. Biol. Chem. 273*, 12259−12266.
13. Dix, T. A., and Benkovic, S. J. (1988) *Acc. Chem. Res. 21*, 101−107.
14. Haavik, J., and Flatmark, T. (1987) *Eur. J. Biochem. 168*, 21−26.
15. Teigen, K., Frøystein, N. Å., and Martínez, A. (1999) *J. Mol. Biol. 294*, 807−823.
16. Almås, B., Toska, K., Teigen, K., Groehn, V., Pfleiderer, W., Martínez, A., Flatmark, T., and Haavik, J. (2000) *Biochemistry 39*, 13676−13686.
17. Erlandsen, H., Bjørgo, E., Flatmark, T., and Stevens, R. C. (2000) *Biochemistry 39*, 2208−2217.
18. Jiang, G. C., Yohrling, G. J., Schmitt, I. V., and Vrana, K. E. (2000) *J. Mol. Biol. 302*, 1005−1017.
19. Schünemann, V., Meier, C., MeyerKlaucke, W., Winkler, H., Trautwein, A. X., Knappskog, P. M., Toska, K., and Haavik, J. (1999) *J. Bioinorg. Chem. 4*, 223−231.
20. Martínez, A., Knappskog, P. M., Olafsdottir, S., Døskeland, A. P., Eiken, H. G., Svebak, R. M., Bozzini, M., Apold, J., and Flatmark, T. (1995) *Biochem. J. 306*, 589−597.
21. Knappskog, P. M., and Haavik, J. (1995) *Biochemistry 34*, 11790−11799.
22. Knappskog, P. M., Flatmark, T., Aarden, J. M., Haavik, J., and Martínez, A. (1996) *Eur. J. Biochem. 242*, 813−821.
23. Flatmark, T., Jacobsen, S. W., and Haavik, J. (1980) *Anal. Biochem. 107*, 71−74.

24. Gottschall, D. W., Dietrich, R. F., Benkovic, S. J., and Shiman, R. (1982) *J. Biol. Chem. 257*, 845−849.
25. Blair, D., and Diehl, H. (1961) *Talanta 7*, 163−174.
26. Martínez, A., Abeygunawardana, C., Haavik, J., Flatmark, T., and Mildvan, A. S. (1993) *Biochemistry 32*, 6381−6390.
27. Dwek, R. A. (1975) *Nuclear Magnetic Resonance in Biochemistry. Application to Enzyme Systems*, Clarendon Press, Oxford, U.K.
28. Liu, M., Mao, X., Ye, C., Huang, H., Nicholson, J. K., and Lindon, J. C. (1998) *J. Magn. Reson. 132*, 125−129.
29. Hwang, T.-L., and Shaka, A. J. (1994) *J. Magn. Reson., Ser. A 112*, 275−279.
30. Lippens, G. (1995) *J. Biomol. NMR 5*, 327−331.
31. Sklenár, V. (1995) *J. Magn. Reson. 114*, 132−135.
32. Campbell, A. P., and Sykes, B. D. (1993) *Annu. Rev. Biophys. Biomol. Struct. 22*, 99−122.
33. Clore, G. M., and Gronenborn, A. M. (1983) *J. Magn. Reson. 53*, 423−442.
34. Clore, G. M., and Gronenborn, A. M. (1998) *Proc. Natl. Acad. Sci. U.S.A. 95*, 5891−5898.
35. Meng, E. C., Shoichet, B. K., and Kuntz, I. D. (1992) *J. Comput. Chem. 13*, 505−524.
36. D'Sa, C. M., Arthur, R. E., and Kuhn, D. M. (1996) *J. Neurochem. 67*, 917−926.
37. D'Sa, C., Arthur, R., Jennings, I., Cotton, R. G. H., and Kuhn, D. M. (1996) *J. Neurosci. Methods 69*, 149−153.
38. Tong, J. H., and Kaufman, S. (1975) *J. Biol. Chem. 250*, 4152−4158.
39. Ichiyama, A., Hasegawa, H., Tohyama, C., Dohmoto, C., and Kataoka, T. (1976) *Adv. Exp. Med. Biol. 74*, 103−117.
40. Yang, X. J., and Kaufman, S. (1994) *Proc. Natl. Acad. Sci. U.S.A. 91*, 6659−6663.
41. Bailey, S. W., and Ayling, J. E. (1983) *Biochemistry 22*, 1790−1798.
42. Mildvan, A. S., Granot, J., Smith, G. M., and Liebman, M. n. (1980) *Adv. Inorg. Biochem. 2*, 211−236.
43. Bertini, I., and Luchinat, C. (1986) *NMR of paramagnetic molecules in biological systems*, The Benjamin/Cummings Publishing Co.
44. Burton, D. R., Forsen, S., Karkstrom, G., and Dwek, R. A. (1979) *Prog. Nuclear Magn. Reson. Spectrosc. 13*, 1−45.
45. Wüthrich, K. (1976) *NMR in Biological Research: Peptides and Proteins*, North-Holland Publishing Co., Amsterdam.
46. Havel, T. F. (1991) *Prog. Biopys. Mol. Biol. 56*, 43−78.
47. Martínez, A., Vageli, O., Pfleiderer, W., and Flatmark, T. (1998) *Pteridines 9*, 44−52.
48. Daubner, S. C., and Fitzpatrick, P. F. (1999) *Biochemistry 38*, 4448−4454.
49. Knappskog, P. M., Eiken, H. G., Martinez, A., Flatmark, T., and Apold, J. (1995) *Hum. Genet. 95*, 171−173.
50. Gámez, A., Pérez, B., Ugarte, M., and Desviat, L. R. (2000) *J. Biol. Chem. 275*, 29737−29742.
51. Ellis, H. R., Daubner, S. C., and Fitzpatrick, P. F. (2000) *Biochemistry 39*, 4174−4181.
52. Jennings, I. G., Cotton, R. G., and Kobe, B. (2000) *Arch. Biochem. Biophys. 384*, 238−244.
53. Yohrling, G. J., IV, Mockus, S. M., and Vrana, K. E. (1999) *J. Mol. Neurosci. 12*, 23−34.
54. Haavik, J., Andersson, K. K., and Flatmark, T. (1989) *Pteridines 1*, 11−16.
55. Haavik, J., Døskeland, A. P., and Flatmark, T. (1986) *Eur. J. Biochem. 160*, 1−8.
56. Friedman, P. A., Kappelman, A. H., and Kaufman, S. (1972) *J. Biol. Chem. 247*, 4165−4173.
57. Hasegawa, H., Oguro, K., Naito, Y., and Ichiyama, A. (1999) *Eur. J. Biochem. 261*, 734−739.
58. Haavik, J., Le Bourdelles, B., Martinez, A., Flatmark, T., and Mallet, J. (1991) *Eur. J. Biochem. 199*, 371−378.
59. Moran, G. R., Derecskei-Kovacs, A., Hillas, P. J., and Fitzpatrick, P. F. (2000) *J. Am. Chem. Soc. 122*, 4535−4541.
60. Kuhn, D. M., and Arthur, R., Jr. (1998) *J. Neurosci. 18*, 7111−7117.
61. Matsubara, K., Ota, M., Takahashi, T., Maruyama, W., and Naoi, M. (1994) *Brain Res. 655*, 121−127.
62. Martínez, A., Dao, K. K., McKinney, J., Teigen, K., and Frøystein, N. Å. (2000) *Pteridines 11*, 32−33.
63. Fauquet, M., Grima, B., Lamouroux, A., and Mallet, J. (1988) *J. Neurochem. 50*, 142−148.
64. Raymer, M. L., Sanschagrin, P. C., Punch, W. F., Venkataraman, S., Goodman, E. D., and Kuhn, L. A. (1997) *J. Mol. Biol. 265*, 445−464.
65. Grenett, H. E., Ledley, F. D., Reed, L. L., and Woo, S. L. (1987) *Proc. Natl. Acad. Sci. U.S.A. 84*, 5530−5534.
66. Neckameyer, W. S., and White, K. (1992) *J. Biol. Chem. 267*, 4199−4206.
67. Adams, M. D., Celniker, S. E., Holt, R. A., Evans, C. A., Gocayne, J. D., et al. (2000) *Science 287*, 2185−2195.

BI015722X